



This is a repository copy of *Determination of sub-resolution structure of jet by solar magnetoseismology*.

White Rose Research Online URL for this paper:

<http://eprints.whiterose.ac.uk/99161/>

Version: Accepted Version

Article:

Morton, R.J., Verth, G., McLaughlin, J.A. et al. (1 more author) (2011) Determination of sub-resolution structure of jet by solar magnetoseismology. *The Astrophysical Journal*, 744 (11). ISSN 0004-637X

<https://doi.org/10.1088/0004-637X/744/1/5>

Reuse

Unless indicated otherwise, fulltext items are protected by copyright with all rights reserved. The copyright exception in section 29 of the Copyright, Designs and Patents Act 1988 allows the making of a single copy solely for the purpose of non-commercial research or private study within the limits of fair dealing. The publisher or other rights-holder may allow further reproduction and re-use of this version - refer to the White Rose Research Online record for this item. Where records identify the publisher as the copyright holder, users can verify any specific terms of use on the publisher's website.

Takedown

If you consider content in White Rose Research Online to be in breach of UK law, please notify us by emailing eprints@whiterose.ac.uk including the URL of the record and the reason for the withdrawal request.

DETERMINATION OF SUB-RESOLUTION STRUCTURE OF A JET BY SOLAR MAGNETOSEISMOLOGY

R. J. MORTON¹, G. VERTH², J. A. McLAUGHLIN², AND R. ERDÉLYI¹

¹ Solar Physics and Space Plasma Research Centre (SP²RC), University of Sheffield, Hicks Building, Hounsfield Road, Sheffield S3 7RH, UK;
r.j.morton@sheffield.ac.uk

² School of Computing, Engineering & Information Sciences, Northumbria University, Newcastle Upon Tyne NE1 8ST, UK; gary.verth@northumbria.ac.uk
Received 2011 June 9; accepted 2011 September 12; published 2011 December 7

ABSTRACT

A thin dark thread is observed in a UV/EUV solar jet in the 171 Å, 193 Å, and 211 Å, and partially in 304 Å. The dark thread appears to originate in the chromosphere but its temperature does not appear to lie within the passbands of the Atmospheric Imaging Assembly onboard the *Solar Dynamics Observatory*. We therefore implement solar magnetoseismology to estimate the plasma parameters of the dark thread. A propagating kink (transverse) wave is observed to travel along the dark thread. The wave is tracked over a range of ~ 7000 km by placing multiple slits along the axis of the dark thread. The phase speed and amplitude of the wave are estimated and magnetoseismological theory is employed to determine the plasma parameters. We are able to estimate the plasma temperature, density gradient, magnetic field gradient, and sub-resolution expansion of the dark thread. The dark thread is found to be cool, $T \lesssim 3 \times 10^4$, with both strong density and magnetic field gradients. The expansion of the flux tube along its length is $\sim 300\text{--}400$ km.

Key words: magnetic fields – magnetohydrodynamics (MHD) – plasmas – Sun: oscillations

Online-only material: color figures

1. INTRODUCTION

Short-lived, transient phenomena are commonplace in the solar atmosphere. In particular, large jet-like features are commonly seen to erupt from the lower to mid-solar atmosphere, ejecting material into the corona. These phenomena are grouped under the term solar jets, which covers a wide range of explosive events that have been observed over the last century, including H α surges (Newton 1934), macro-spicules (Bohlin et al. 1975), UV/EUV (Brueckner & Bartoe 1983), X-ray jets (Shibata et al. 1992), and solar tornadoes (Pike & Mason 1998).

It is believed that these events are driven by relatively localized reconnection events (e.g., Yokoyama & Shibata 1995, 1996; Harrison 1999), where emerging magnetic flux reconnects with existing fields. One feature that has been reported a number of times among the jets seen in UV/EUV is a large-scale torsional/helical motion (e.g., Shimojo et al. 1996; Pike & Mason 1998; Patsourakos et al. 2008; Liu et al. 2009; Kamio et al. 2010). Proposed reconnection models suggest that closed twisted field lines reconnect with surrounding open field lines (e.g., Shibata & Uchida 1985; Pariat et al. 2009).

Whatever the exact excitation mechanism of these jets is, it appears to coincide with the excitation of a number of different types of wave phenomena. First, there is the large-scale torsional/helical motion reported in both observations (e.g., Kamio et al. 2010) and simulations (e.g., Pariat et al. 2009), whose interpretation is still in debate (the candidates being torsional Alfvén waves (e.g., Pariat et al. 2009), or helical kink waves (M. S. Ruderman 2011, private communication)). The second type of reported wave phenomena is the transverse (kink) wave (Cirtain et al. 2007; Liu et al. 2009). However, in the majority of observations of transverse (kink) waves in jets, the wave phenomena, in our view, was wrongly interpreted as an Alfvén wave, whose features are quite distinct from the transverse kink wave (Erdélyi & Fedun 2007; Van Doorsselaere et al. 2008). The transverse kink waves are normally reported in a bright, fast moving part of the jet which is common to the X-ray jets.

The study of wave phenomena in the solar atmosphere proves useful as demonstrated by the new and expanding field of solar magnetoseismology, which exploits observed wave phenomena to determine hard to measure or unmeasurable plasma parameters (Uchida 1970; Roberts et al. 1984; Erdélyi 2006a, 2006b). Recent advances in observing technology has demonstrated the ubiquitous nature of waves in the solar atmosphere (see, e.g., Banerjee et al. 2007; Andries et al. 2009; De Moortel 2009; Ruderman & Erdélyi 2009; Taroyan & Erdélyi 2009, for reviews of waves in the solar atmosphere). However, magnetoseismology has largely been confined to observations of structures with relatively long lifetimes, e.g., coronal loops, (e.g., Taroyan & Bradshaw 2008; Verth et al. 2008; Taroyan & Erdélyi 2009; Morton & Erdélyi 2009a, 2010; Verth et al. 2010; Terradas et al. 2011), prominences (e.g., Pintér et al. 2008; Soler et al. 2010), although recent papers have extended solar magnetoseismology to transient events such as X-ray jets (Vasheghani Farahani et al. 2009), coronal waves (West et al. 2011), and spicules (Zaqarashvili & Erdélyi 2009; Verth et al. 2011).

Why should magnetoseismology be used to study solar jets? One reason is that jets are short-lived events with even shorter lived components, e.g., associated spicule-like features at the footpoints (Sterling et al. 2010). Regular methods of determining plasma properties, e.g., magnetic field gradients by spectropolarimetry, can require fairly long integration times. For example, Centeno et al. (2010) attempted to measure spicule magnetic field strengths. However, large signal-to-noise ratios in off-limb measurements meant integration times of 45 minutes. Spicules exist only for 5–15 minutes (Zaqarashvili & Erdélyi 2009) so such measurements are much longer than the lifetimes of the objects they are trying to study. Another reason is that properties of dark features, i.e., little or no intensity at certain wavelengths, cannot be measured from the spectral information at those wavelengths. Solar magnetoseismology negates these difficulties as the changing properties of the wave, i.e., period, phase speed, amplitude can reveal the required information on plasma stratification properties, i.e., magnetic field gradient,

density scale heights, etc. This approach has been demonstrated successfully by Verth et al. (2011) in the study of spicules. Further to this, solar jets are multi-thermal (Kamio et al. 2010). X-ray jets in particular have a rapid, hot ejection of material seen in X-rays and a much cooler ejection of material that makes up the jet observed in EUV lines (see, e.g., Kamio et al. 2010). Obtaining values of plasma parameters, e.g., temperature, and variation of plasma parameters with height, e.g., density, magnetic field, of multi-temperature features from the spectroscopic data available in the narrowband filters, such as those onboard the *Solar Dynamics Observatory* (*SDO*), proves difficult if not impossible. Solar magnetoseismology, again, negates this problem. For example, magnetoseismology can be used to determine the density and magnetic field gradients, and temperature, in theory, of a feature that appears dark in an *SDO* filter. Little or no information could be obtained about the plasma in the object of interest from the filter response itself. Finally, magnetoseismology allows the determination of fine structure at sub-resolution scales. It is at these small scales that wave heating may occur, so the study of such length scales is vitally important.

In the following, we present the observations of a propagating kink wave observed in a structure associated with a solar (UV/EUV) jet. The structure is a dark inclusion, in a relatively hot jet, whose presence appears not to have been seen before (at least in EUV lines). We then use magnetoseismology to estimate the temperature, the density stratification, and expansion of the observed magnetic structure. We compare the obtained results with the measured features of the larger jet structure, magnetic field extrapolations for the quiet-Sun magnetic field and chromospheric estimates.

2. OBSERVATIONS

2.1. Solar Jet

The observations began at 09:00 UT on the 2011 January 20 and last an hour and a quarter till 10:15 UT, on the southwest limb using the Atmospheric Imaging Assembly (AIA; Lemen et al. 2011) onboard *SDO* which has a spatial resolution of ~ 0.6 arcsec per pixel or two-pixel spatial resolution of ~ 870 km and a cadence of ~ 12 s. The solar jet was observed mainly in the 304 Å spectral line with faint emission signatures in 171 Å, 193 Å, and 211 Å, close to the southern polar coronal hole. The time series were obtained from the SolarSoftWare (SSW) cutout service which provides level 1.5 data that has already been corrected for flat-field, despiked, and the images co-aligned. The line in which the jet appears brightest is the 304 Å which has a peak temperature of $\sim 10^{4.7}$ K (see first row in Figure 1). Our main interest lies in a dark thread in the 171 Å line (second row in Figure 1); however, we will also describe the part of the jet seen in the 304 Å channel as it will be important later.

In Figure 1, we also provide images from the Sun Earth Connection Coronal and Heliospheric Investigation (SECCHI) telescopes onboard the *Solar Terrestrial Relations Observatory* (*STEREO*; Howard et al. 2008) to show the orientation of the jet in the line of sight with respect to *SDO* (third and fourth rows). The bright UV/EUV portion of the jet has a $\sim 18^\circ$ angle with the normal to the Sun's surface; however, it is not possible to determine the angle between the dark thread and this normal. If it is similar to the UV/EUV jet then any projection effects should be relatively small but should be kept in mind. There is also a clear emission in the 171 Å filter from the jet, which appears as a relatively distinct spike in the quiet corona. The EUV emission

is relatively dim suggesting the bulk of the material in the jet is less than 1 MK, although due to blending of the 171 Å with cooler lines the actual value could be significantly less than this (see, e.g., Del Zanna & Mason 2003).

The jet occurs close to the limb at the southern pole of the Sun and is situated just outside a coronal hole in a relatively quiet region. We do not go into a detailed discussion here of how the jet may be driven; however, one possible scenario is the jet could be generated by a reconnection event in the lower solar atmosphere. This will be the subject of a further investigation. In Figure 1, we show the morphology of the jet over its lifetime at various times.

In the 304 Å line, we see a small bright collimated jet rise from the surface. The jet expands with height and time and during its main phase, highlights a funnel shape. We place cross-cuts of 70 pixels in length and 1 pixel in width perpendicular to the central axis of the jet at heights of ~ 10 Mm, ~ 14.3 Mm, and ~ 15.7 Mm above the limb and use linear interpolation to obtain an $x-t$ dataset. We then measure the width expansion of the jet over time at various heights as a function of time, Figure 2(a). (N.B. in all figures from now on the times are given in seconds from 9:22 UT, which is when the kink wave is first observed. The benefit of this is clear in Section 4 on magnetoseismology.) The jet is clearly defined due to the jet material having a much greater intensity than the surrounding chromospheric material and the jet edges are determined by eye. We suggest there could be an error of $\leq 10\%$ on these measurements. Figure 2(a) shows that there is a similar trend for the expansion of the jet over time at all heights. As certain reconnection scenarios involving reconnection between emerging and existing field describe an untwisting magnetic field, it is possible that the expansion of the jet cross-section in time is partly due to the untwisting of the field. The expansion of the flux tube in Figure 2(a) is not constant but goes through a number of phases.

At around 16 Mm above the surface the jet experiences a whip-like effect (see Figure 1) similar to that reported in Liu et al. (2009). The plasma above the whip appears collimated. Once the plasma has finished being ejected into the atmosphere, a portion of it returns to the surface. This falling material highlights the magnetic field and it follows a collimated path back to the chromosphere suggesting the complete untwisting of the magnetic field has occurred. The funnel shape of the magnetic field has now evolved into a column.

Further to this, we calculate the median value of intensity flux, F , in the 304 Å channel of the pixels in the cross-cut placed at 10 Mm, which were determined to lie within the jet boundaries. This is plotted as a function of time in Figure 2(b). We do this because the intensity is dependent upon thermodynamic quantities, e.g., temperature and density, so provides an estimate of how the density/temperature in the jet evolves as a function of time.

In the 171 Å channel, the jet appears completely different to that seen in 304 Å. At 09:16, a bright loop is clearly seen with the eruption starting two minutes after. A thin, dark thread, with a width at resolution scales, is then seen to be ejected into the atmosphere along with a very small amount of bright material. The dark material appears to come from the chromosphere, appearing (apparently) from behind the bright loop (09:18) (Figure 1). This is the first appearance of the dark thread that is shown in the image at 09:25. The dark thread is co-spatial and co-temporal with the UV/EUV component of the jet in the 304 Å channel but is barely visible among the hotter plasma. In the middle right panel of the 304 Å images a bright, thin

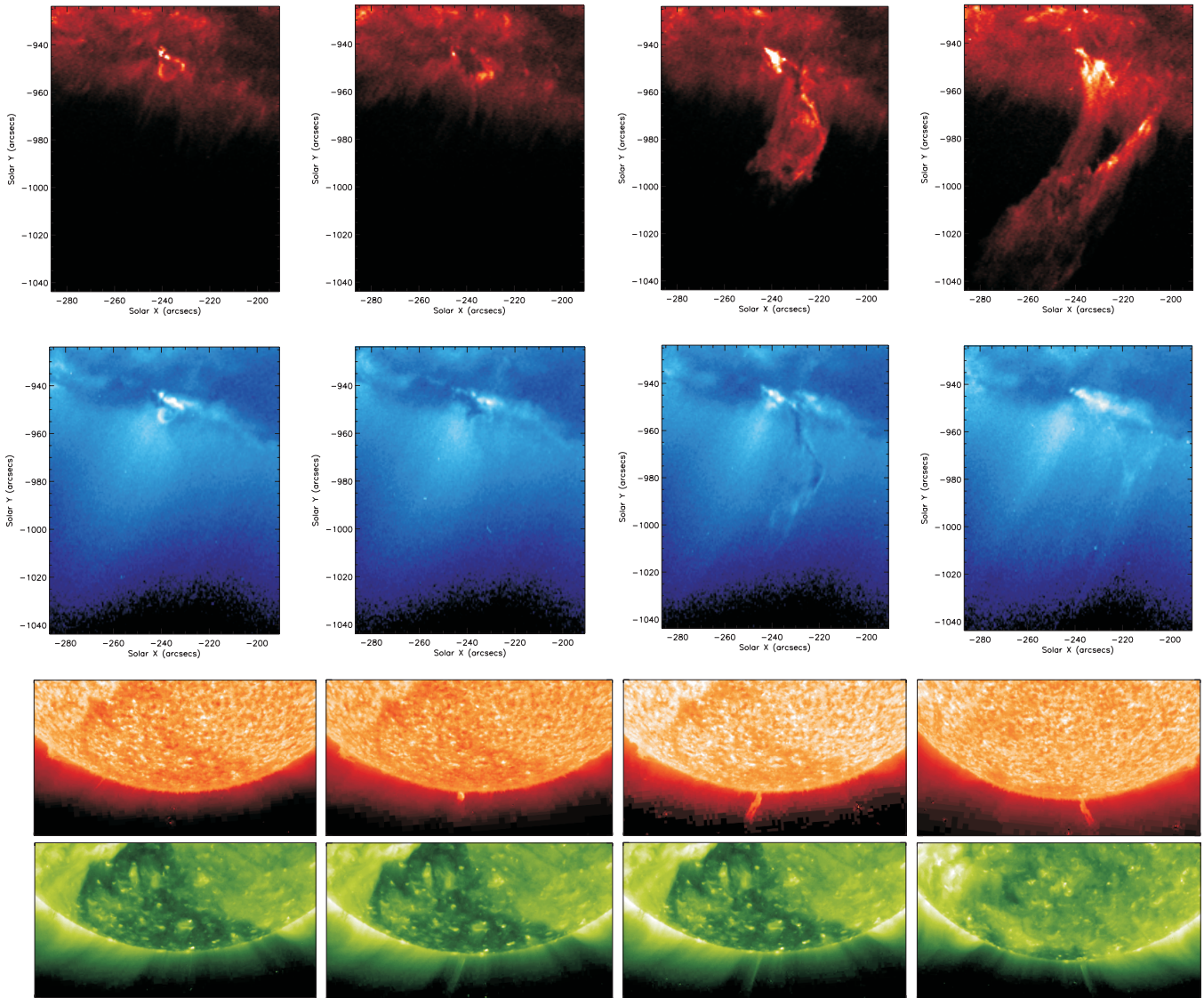


Figure 1. First and second rows: images showing the morphology of a large jet (observed on 2011 January 20) over its lifetime taken by *SDO/AIA*. The panels in the top row are from the 304 Å channel taken at 09:16, 09:18, 09:25, and 09:33. The images on the bottom row are from the 171 Å channel taken at the same times. The bright loop is seen in both channels at 09:16, suggestive of reconnection. A dark feature is seen at 09:18 at the same position as the bright loop appeared. This dark feature grows into the dark thread seen in 171 Å at 09:25. Third and fourth rows: context images of the jet from *STEREO*. The first three panels in each row are from *STEREO A* and the last is from *STEREO B*. The top row are images from the EUVI 304 Å channel and are taken at 09:06, 09:26, 09:36, and 09:36. The bottom row are images from the EUVI 171 Å channel and are taken at 09:03, 09:28, 09:33, and 09:33.

(A color version of this figure is available in the online journal.)

thread of plasma is seen to highlight the right-hand jet edge. This can just be made out in the corresponding 171 Å image running along the right-hand side of the dark thread. Toward the base of the bright thread in the 304 Å, a small dark inclusion can be seen which is the dark thread (e.g., third panel, top row, Figure 1). This suggests that the thin, dark thread is a flux tube (or flux tubes) contained within a large collection of flux tubes, i.e., the jet seen in the 304 Å channel. The dark thread survives for around 10 minutes before the material either traveling higher into the atmosphere or returning to the surface. Further, the dark thread jet has an angle of $\sim 35^\circ$ to the normal from the solar surface. The plane in which this angle is measured, i.e., the plane of view of *SDO/AIA*, is almost perpendicular to the plane of view of *STEREO*. Hence, the angle measured for the bright part of the jet in *STEREO* is measured in a different plane to this angle.

Aside from the dark thread, only a small amount of bright plasma is seen to be ejected into the atmosphere in 171 Å. This suggests that the density and/or temperature of the dark thread plasma must be different from the material seen in the 304 Å channel. Due to its appearance as a dark inclusion, we suggest the material is much cooler and/or denser (hence, optically thicker) than the other jet material. The peak sensitivity of the 304 Å channel is $T \sim 10^{4.7}$ K, so the material in the dark thread must be at least $T < 5 \times 10^4$ K. This, along with the appearance of the bright loop at the jet footpoint, supports the popular conjecture that the reconnection event responsible for the jet occurred at chromospheric heights. The dark thread could be similar to the cool chromospheric jet observed by Liu et al. (2009). One difference between the jet observed here and that in Liu et al. (2009) is that the ejected material in Liu et al. (2009) returns to the surface along a similar path to that of its ejection.

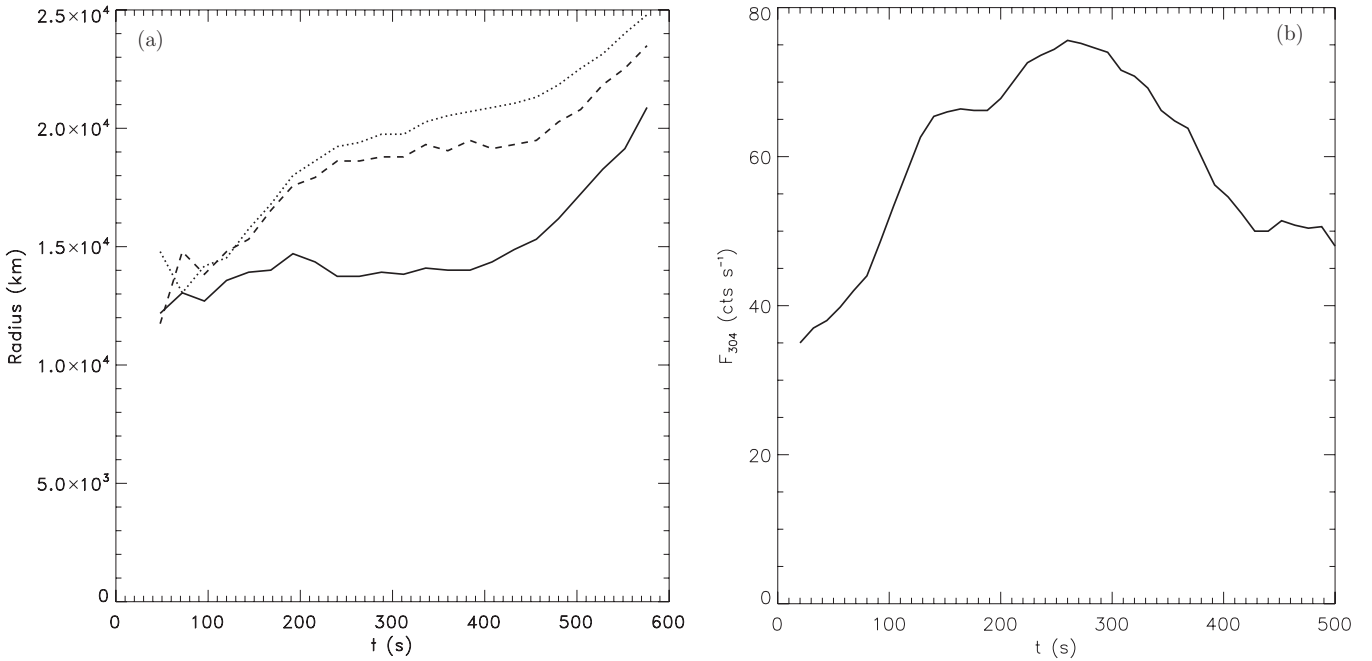


Figure 2. (a) Expansion of the jet width in 304 Å as a function of time plotted for different heights along the jet. The solid line is taken at 11 Mm from the base, the dashed line 14 Mm, and the dotted line 15 Mm. The time is given in seconds from 09:22 UT. (b) Average intensity of the jet in a cross-cut taken at a height of 10 Mm above the solar surface as a function of time in 304 Å. The flux is measured in terms of the number of photon counts per second.

Here, some of the material is ejected higher into the atmosphere while the rest returns to the surface along a different path at least a few Mm from the ejection site.

The dark thread has a width close to the resolution limit so the expansion that is measured for the UV/EUV jet structure is not seen in the dark thread. The outflow of the dark thread material is also a lot slower than outflow of bright material seen in the 171 Å. In 171 Å, we can measure the speed of the outflow for the dark thread by using two methods. For the initial rise of the dark feature, we use a running difference movie to track the dark thread front and obtain average rise speeds of 63 km s^{-1} . After the initial rise we employ a method of contouring features of different intensity and tracking the intensity features through the images (see, e.g., Winebarger et al. 2001, for details). The flow in the dark thread is given as an average speed along the thread of the different intensity features identified and tracked through the thread. Here, we term the initial rise or possible “extension” of the dark thread as outflow. In the following section, we need to subtract any apparent motion, both flow and extension, from measured phase speeds. We use the term outflow to describe the observed upward motion of plasma, making no definite distinction between possible extension and flow.

In Figure 3, we show the outflow speeds along the dark thread as a function of time. The speed of the outflow lies within the range of outflow speeds reported in Liu et al. (2009). We then smooth the measured values of flow with a five-point boxcar average and fit a quadratic profile to the smoothed points which is the dash-dotted line in Figure 3. It would appear that there are two distinct phases to the flow; a phase with decreasing flow speed and a phase of almost constant flow speed. Separating these into two different phases we construct quadratic fits to the two phases (solid lines). The second phase can be seen to have an almost constant flow speed. It is unknown why the outflow rate appears to have these two distinct phases, but is probably connected to the nature of the explosive (reconnection) event.

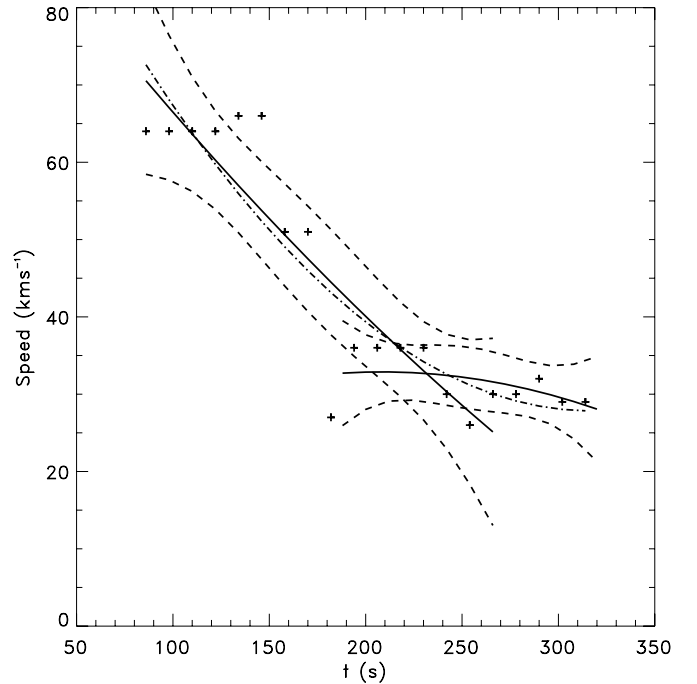


Figure 3. Measured values of flow as a function of time along the dark thread in the 171 Å. The crosses are the measured values while the solid lines correspond to the quadratic fits to the measured values smoothed with five-point boxcar average. The dashed lines are the 95% confidence levels from the fits. The dash-dotted line is a quadratic fit to all the data points.

2.2. Transverse Wave

We can determine very little about the dark thread from the *SDO* filters due to its low intensity in all *SDO* filters. However, we observe a propagating transverse wave traveling along the thread. The natural interpretation for the wave is a propagating transverse wave (propagating kink wave). A number of previous

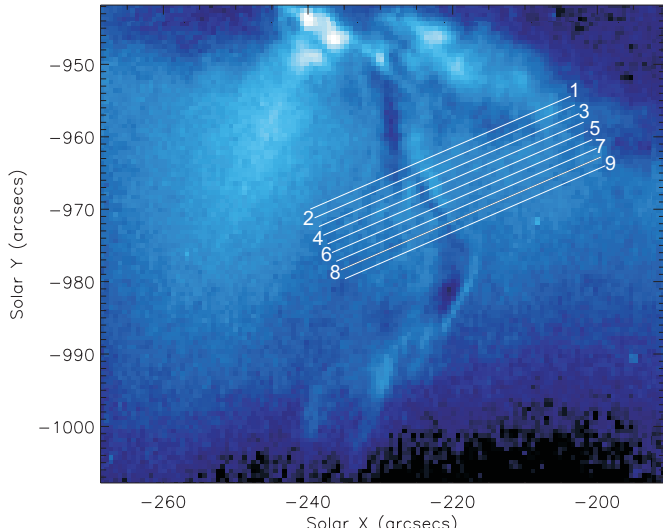


Figure 4. Image of the dark thread showing the cross-cut positions. The observed transverse motion propagates from cross-cut 1 to 9.
(A color version of this figure is available in the online journal.)

authors have reported observed displacements of the jet axis as the Alfvén wave. However, Alfvén waves are oscillations of constant magnetic surfaces and do not displace the flux tube axis, the only mode that causes a visible displacement of the flux tube axis is the kink mode (see, e.g., Erdélyi & Fedun 2007; Van Doorsselaere et al. 2008, for discussion). The transverse wave should allow us to estimate certain plasma parameters by means of solar magnetoseismology. First, in this subsection we describe how we obtain the information about the wave and in the following sections we discuss the magnetoseismology.

We determine the line parallel to the final axis of the dark thread and then place nine cross-cuts (linearly interpolated) perpendicular to the line, with the cross-cuts separated by 0.97 Mm (see Figure 4). The wave appears at approximately half-way along the thread, which is approximately ~ 7 Mm above the limb in 171 Å. We do not consider projection effects along the line of sight for estimates on distances and heights. The angle between the normal to the solar surface and the UV/EUV jet is approximately $\sim 18^\circ$ (see Figure 1), so the correction will only be relatively small, $\sim 5\%$ on measured distances. The propagating kink wave can be seen up to a height of ~ 15 Mm in the atmosphere. This corresponds to the wave traveling a distance of ~ 11.6 Mm along the dark thread. An example of the oscillation observed in one of the cross-cuts is shown in an x - t plot in Figure 5(a).

To obtain information about the wave, we determine the pixel in each time frame of the x - t plot that has the minimum intensity. The dark thread has an almost inverse Gaussian intensity profile across its width and the minimum intensity should correspond closely to the minimum of this inverse Gaussian. We then smooth the data points of the oscillation using a five-point boxcar function before applying a linear fit to the smoothed data. The linear fit is subtracted from the smoothed data to remove the trend. An example of these steps is demonstrated in Figures 5(b) and (c). We then determine the times at which the zero crossings and the maximum and minimum values of amplitudes occur in the different cross-cuts. The magnitude of the maximum and minimum values of the amplitudes is also determined. Above the ninth cross-cut the strength of the wave signal is weak making it difficult to obtain fits to the observed profile. We

begin by plotting the travel times at which the zero crossings and the maximum and minimum values of amplitudes occur at the different heights in Figure 6(a). The cross-cut labeled no. 1 in Figure 4 is the first cross-cut in which we see the oscillation; hence, in Figure 6(a) we measure distance from this cross-cut. The crosses correspond to the values taken from the observations and the lines correspond to a quadratic fit to the data points of each feature. The gradient of the quadratic fits gives the speeds at which the zero crossings and the maximum and minimum values of amplitudes travel along the dark thread and is shown in Figure 7(a).

One might expect that the speeds of each point should have similar behavior as they propagate to the different heights. However, as we have illustrated in Figures 2 and 3, the plasma properties, i.e., flow, magnetic field and density, in the larger collection of flux tubes (304 Å jet) and the dark thread are subject to large changes over the lifetime of the jet/thread. If we assume a linear fit so that the phase speeds are constant, we see the trend is a decrease in the phase speed over time. This appears natural as the phase speed of the transverse wave is proportional to the magnetic field, so an untwisting field would decrease the field strength, hence, the value of phase speed will also decrease. N.B. Neglecting inclination of the flux tube with respect to the normal to the solar surface gives errors of ± 3 km s $^{-1}$ which lie well within the errors/confidence levels given by the fitting procedure.

Finally, we plot the size of the maximum and minimum amplitude envelopes in Figure 6(b). It is seen from the amplitude envelope plot initially there is an increase in amplitude with height followed by a decrease. The confidence intervals on the fits demonstrate that there is a possibility that the amplitude does not necessarily have to be decreasing after 4000 km. It is clear from the confidence intervals in Figure 6(b) that the minimum amplitude appears to have large errors associated with it. In the following sections we will use only the maximum amplitude envelope to increase confidence in our results.

3. THEORY

Before we analyze the wave motion any further we need to determine which, if any, theory already developed is relevant to these observations. A complete theory that would describe kink motion in the jet scenario has not yet been fully developed due to the immense complication associated with including all the topological and dynamic features that the reported jet possess. However, we will assume static behavior and adapt the theory for a magnetic flux tube with both magnetic and density stratification (Verth & Erdélyi 2008; Ruderman et al. 2008). If the plasma is indeed cool as we suspect, then it may be better to use models including a partially ionized plasma, e.g., Soler et al. (2009a, 2009b) who model prominence plasmas. However, the results from these models indicate partial ionization, at least in single fluid theory, has a small effect on the propagation and damping of kink oscillations (for typical observed wavenumbers).

First, we need to make sure any assumptions used in the derivations of the previous theories are also adequate for this dark thread: (1) the thin tube approximation applies. For this, we require the wavelength of the oscillation to be much greater than the radius. The width of the dark thread is measured to be < 500 km. We can estimate the wavelength/wavenumber of the kink wave. The typical period of the oscillations (e.g., see oscillation in Figure 5) is 360 s. Using $P = 2\pi/\omega = \lambda/c_k$ and values of phase speed from Figure 7(b) then, $5400 < \lambda <$

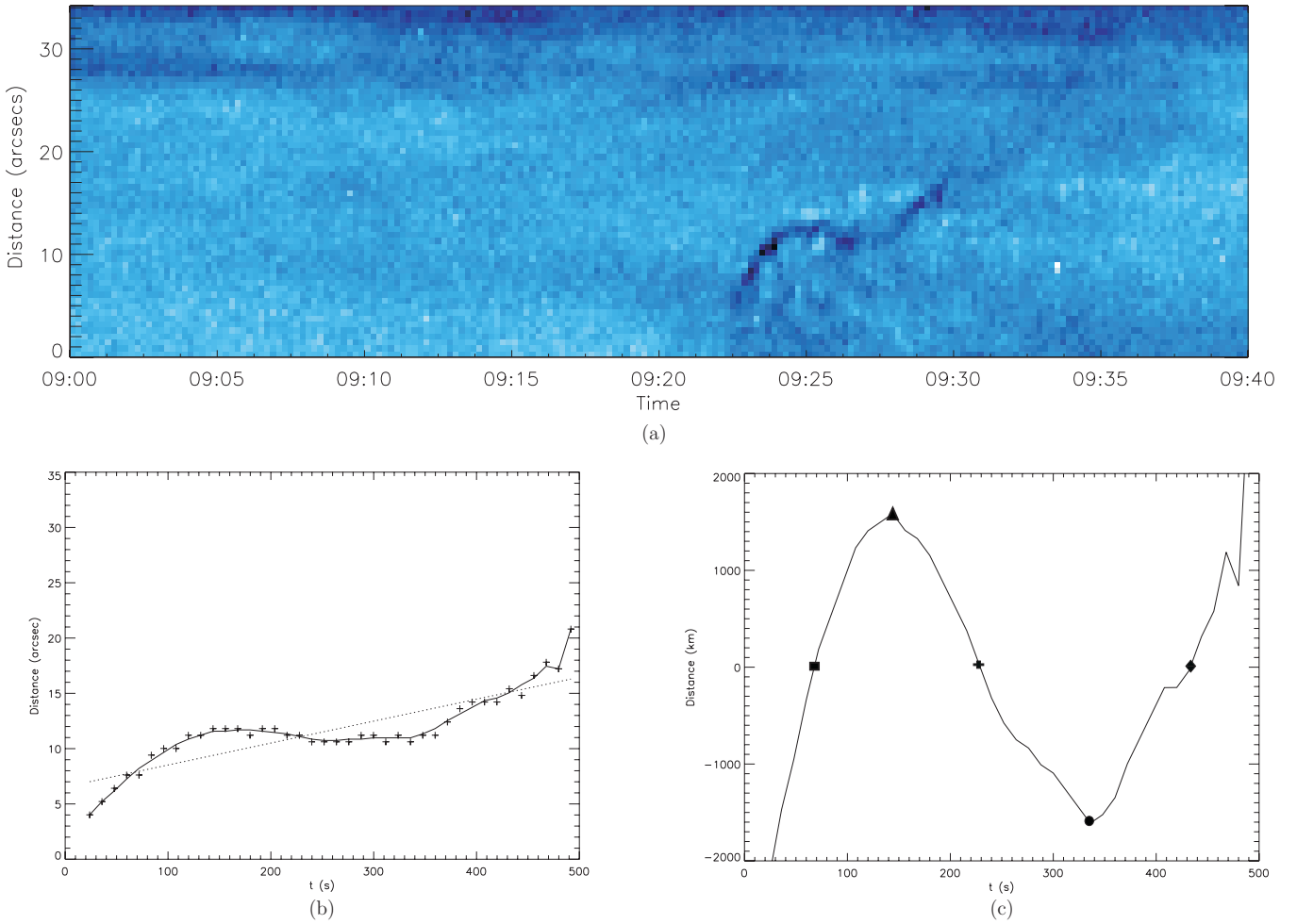


Figure 5. (a) Sample cross-cut x - t plot (cross-cut no. 3). The transversal kink motion of the dark thread is clearly seen. (b and c) An example of the fitting procedure for the third cross-cut. (b) The middle panel shows the data points (crosses) over plotted with a smoothed profile (solid line). The dotted line shows the linear fit to the wave. (c) The right-hand panel shows the wave with the linear fit subtracted. The symbols indicate the first zero crossing (square), the maximum (triangle), the second zero crossing (cross), the minimum (circle), and the third zero crossing (diamond).

(A color version of this figure is available in the online journal.)

18,000 km and hence $R/\lambda \lesssim 0.1$. (2) The plasma- β is small. Estimates for the sound speed in the chromosphere are in the range 5–12 km s $^{-1}$ ($T = 5 \times 10^4$ – 1×10^5 K) while the Alfvén speed is between 50 and 200 km s $^{-1}$. The plasma- β is given by $\beta = 2c_s^2/(\gamma v_A^2)$ so estimates for the jet give $\beta < 0.25$. From these estimates we can consider the plasma- β in the dark thread to be small. (3) The plasma inside the dark thread is much denser than the surrounding material, i.e., $\rho_i \gg \rho_e$. Although this is not a necessary condition, it allows simplification of the governing equations and suggests that the properties of the internal plasma dominate the wave behavior. The dark thread appears to originate from the chromosphere/transition region and ejects the material from these regions high into the corona. It is generally well accepted that corona is much less dense than the lower layers of the solar atmosphere; hence, ρ_i is at chromospheric/transition region densities and ρ_e is at coronal densities. However, the plasma at UV/EUV temperatures in 304 Å appears to surround the dark thread, so the external plasma could be considered to be at upper chromosphere/transition region temperatures and densities. It is then much less clear whether ρ_e is less than ρ_i .

First, the phase speed for a kink (or transverse) mode in a thin tube is given by

$$c_k(z, t) = \left(\frac{B_i(z, t)^2 + B_e(z, t)^2}{\mu_0(\rho_i(z, t) + \rho_e(z, t))} \right)^{1/2}, \quad (1)$$

where the subscripts i and e refer to the internal and external values of the plasma quantities. Instead of making any assumptions about the relative magnitudes of the densities and magnetic field we will rewrite this in terms of the average density and magnetic field

$$c_k = \frac{B}{\sqrt{\mu_0\rho}}, \quad (2)$$

where $\rho = (\rho_i(z, t) + \rho_e(z, t))/2$ and $B^2 = (B_i(z, t)^2 + B_e(z, t)^2)/2$.

Now, in Ruderman et al. (2008) the kink wave equation for a magnetostatic flux tube with both magnetic and plasma density stratification in the longitudinal direction is given by

$$\frac{d^2\eta}{dz^2} + \frac{\omega^2}{c_k^2(z)}\eta = 0, \quad (3)$$

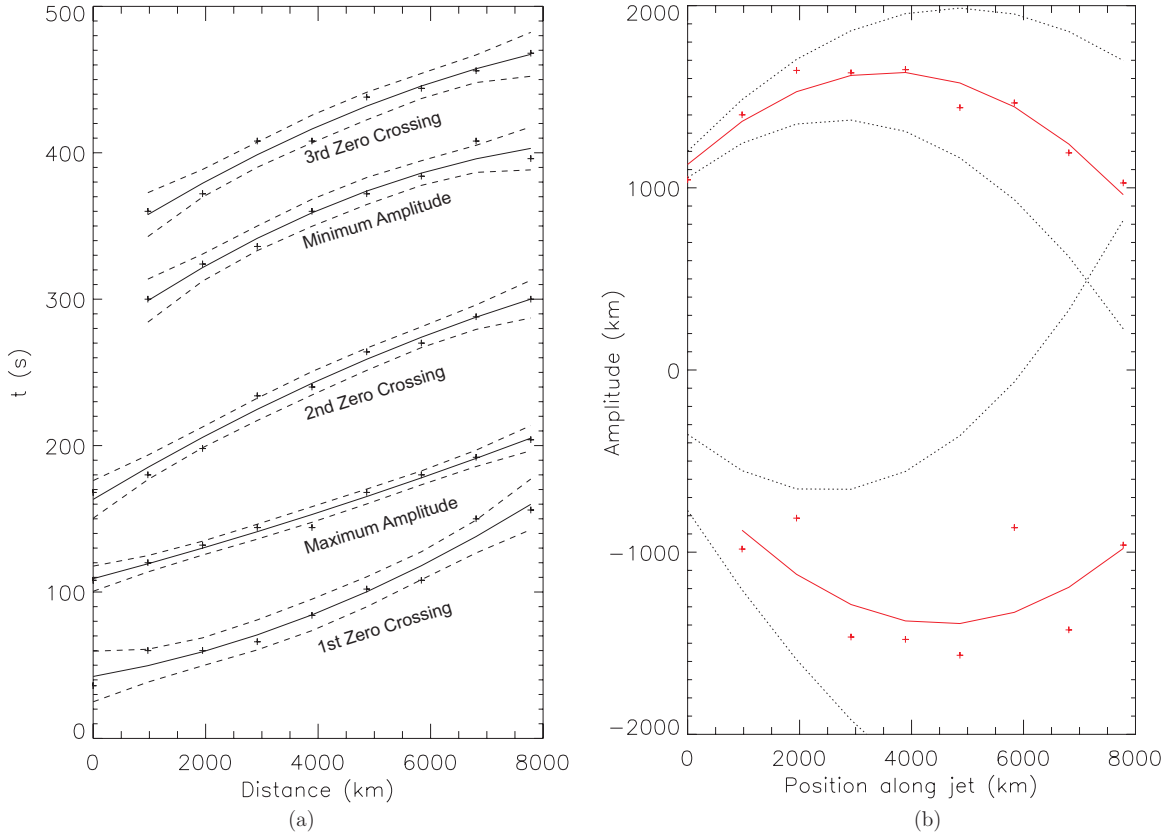


Figure 6. (a) Shown are the times at which the zero crossings and maximum and minimum amplitudes appear at the different heights (cross-cuts). The data points (crosses) have been fitted with a quadratic profile (solid line) and the 95% confidence interval is shown for the fit. (b) Maximum and minimum values of the amplitude envelope plotted as a function of height. The crosses correspond to the measured values, the solid line is a quadratic fit to the data points, and the dashed lines correspond to a sigma confidence interval for fit to the maximum amplitude envelope and 0.5 σ confidence interval for fit to the minimum amplitude envelope.

(A color version of this figure is available in the online journal.)

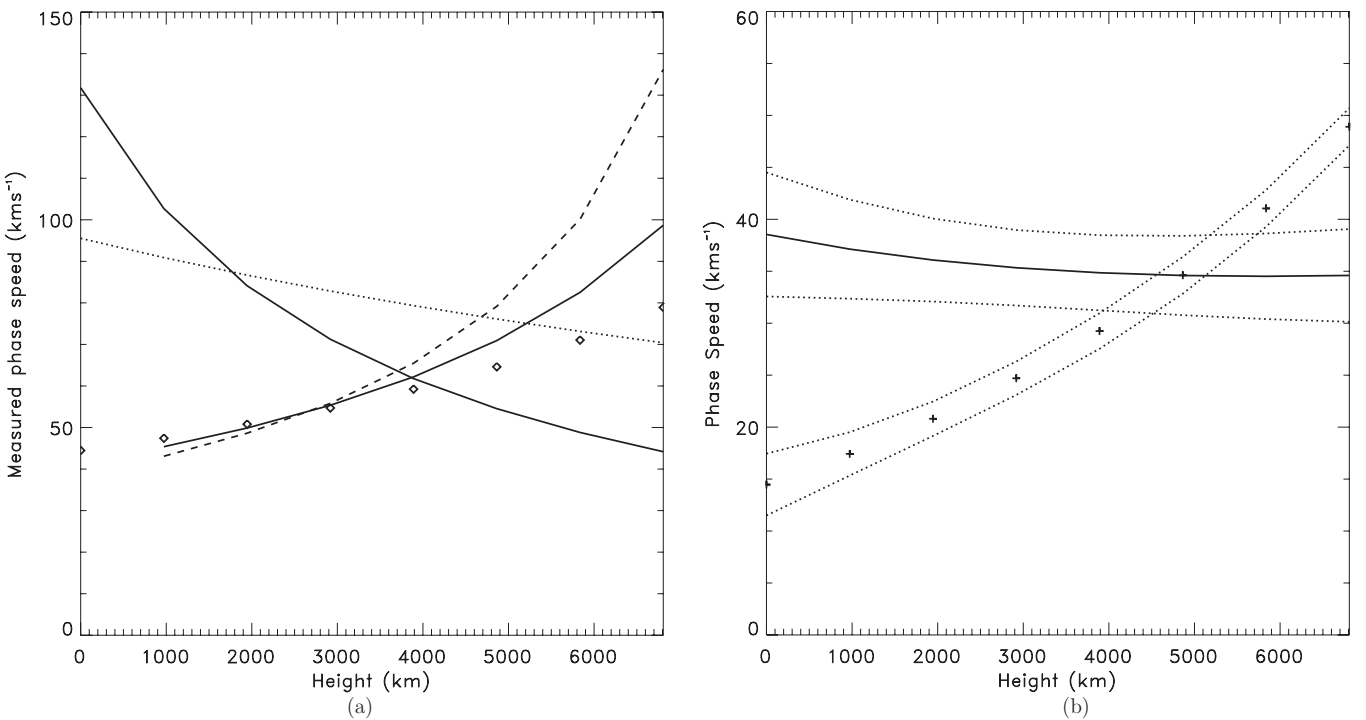


Figure 7. (a) Phase speeds for first zero (solid), maximum amplitude (dotted), second zero (diamonds), minimum amplitude (dashed), and third zero (dashed dot). (b) Measured phase speed minus the measured flow for the maximum amplitude (solid line) and second zero crossing (crosses). The dashed lines correspond to the sigma value error on the phase speeds.

where $\eta = \xi_{\perp}/R(z)$, ξ_{\perp} is the displacement perpendicular to the magnetic field, $R(z)$ is the loop radius, and ω is the frequency of the transverse oscillation.

First, we introduced a scaled length, $\zeta = \epsilon z$ under the assumption the length scale of the changes in the background plasma parameters, i.e., density, magnetic field, are small compared to the wavelength, hence, the kink speed changes slowly along a stratified and expanding waveguide. We now apply the WKB approximation (see, e.g., Bender & Orszag 1978) in the z -direction, assuming that

$$\eta = A(\zeta) \exp(-i\epsilon^{-1}\Theta(\zeta)). \quad (4)$$

Substituting Equation (4) into (3) and taking the zeroth-order terms, with respect to ϵ , gives the frequency

$$\omega = c_k(z)k, \quad (5)$$

where $k = d\Theta/d\zeta$. The first-order terms provide an equation for the amplitude of the wave, namely,

$$\frac{A'}{A} = -\frac{k'}{2k}, \quad (6)$$

where the dash corresponds to derivative with respect to ζ . Solving this and using our definition of η we obtain

$$\xi_{\perp} = \sqrt{\frac{c_k(z)}{\omega}} R(z). \quad (7)$$

The frequency is independent of the changes in the spatial direction, hence, if we can determine the change in phase speed and spatial displacement of the thread (amplitude) with height then the expansion along the flux tube can be calculated.

4. SOLAR MAGNETOSEISMOLOGY

Now, the data we have determined from the observations contain a large amount of information. To demonstrate the magnetoseismology here we shall only use two of the obtained phase travel times, for which the reasons will become clear.

First, we return to the plot of the phase speeds shown in Figure 7(a). For a propagating wave in a flowing medium, the measured phase speed will be a sum of the kink speed and the flow speed (if the wave is propagating in the same direction as the flow). If we subtract the measured value of flow from the measured phase speeds then we see that the actual phase speeds cover a much smaller range of values (e.g., see Figure 7(b)). From Equation (1) we can see the kink speed is also dependent upon the magnetic field and the density. The dynamic changes observed in the large jet could also be occurring in the dark thread and could be sufficient to explain the remaining differences between the phase speeds.

4.1. Scale Height and Temperature Estimates using the Phase Speed

The UV/EUV jet is clearly highly dynamic, where magnetic field and density undergo rapid changes. However, if we consider Figure 2, we can see that there is a period of time when the time-dependent expansion and change in intensity of the jet is at a minimum ($t \approx 170$ s to $t \approx 400$ s). In this period of time, the total expansion of the jet is $\lesssim 5\%$ and the change in intensity is $\lesssim 10\%$. For this time period, the second zero crossing is propagating along the thread. We then make the assumption

that the activity in the dark thread is also at a minimum at this point. If this is the case, the change we see in phase speed at the different heights is due only to the structuring along the thread and not due to dynamic behavior. The second zero crossing appears first at around 156 s (9:24:30 UT), propagates along the cross-cuts within 110 s and experiences an increase in phase speed as it travels along the thread. Using the estimate of flow speed along the jet during this period (Figure 3) we subtract flow from the measured phase speed to obtain the kink speed estimate (Figure 7(b)).

Now, since we have no information on the expansion of the dark thread with height we make the initial assumption that the magnetic field is constant with height. This assumption is only for ease of calculation and provides an upper bound on the density scale height. As will be demonstrated in the next section, this assumption is not necessarily valid in such solar waveguides.

First, we assume the density is gravitationally stratified, such that

$$\rho \propto \exp\left(-\frac{z}{H_{\text{eff}}}\right), \quad (8)$$

where $H_{\text{eff}} = H/\cos\theta$ is the effective density scale height due to the inclination of the dark tube from the normal to the surface (see, e.g., Aschwanden 2004), H is the density scale height, and θ is the inclination angle. We need the relationship

$$\left(\frac{c_{k0}}{c_k}\right)^2 = \frac{\rho}{\rho_0} = \exp\left(-\frac{\Delta z}{H_{\text{eff}}}\right), \quad (9)$$

where the subscript 0 refers to the “first” value of phase speed and density and Δz is the difference in height between where c_{k0} and c_k are measured. Substituting in the obtained values of phase speed for the second zero crossing with flow subtracted (Figure 7(b)), where c_{k0} is the phase speed at height 0 km and c_k is at height 7000 km, we obtain that $H_{\text{eff}} = 2.4 \pm 0.5$ Mm corresponding to $T \sim 0.05 \pm 0.01$ MK, where we have used the relationship

$$H = \frac{2k_B}{\mu m_H g} T, \quad (10)$$

and k_B is the Boltzmann constant, μ is the mean molecular mass, m_H is the mass of hydrogen, and g is the gravitational acceleration ($2k_B/\mu m_H g \approx 47$ Mm MK $^{-1}$; see, e.g., Aschwanden 2004).

We can attempt to take into account expansion with height, which gives a new relationship between phase speed and scale height, namely,

$$\left(\frac{c_{k0}}{c_k}\right)^2 = \frac{B_0^2 \rho}{B^2 \rho_0} = \frac{R^4}{R_0^4} \exp\left(-\frac{\Delta z}{H_{\text{eff}}}\right). \quad (11)$$

Using the values of expansion in the measured range for the larger UV/EUV jet, i.e., $R/R_0 \sim 1.35$ (from Figure 2(a)), and the same values of phase speed for the second zero crossing, we obtain $H_{\text{eff}} = 1.6 \pm 0.5$ Mm corresponding to $T \sim 0.03 \pm 0.01$ MK. Any larger value of expansion for the dark thread will give even smaller values of H and T , hence, assuming no magnetic field expansion along the thread provides an upper bound for density scale heights and temperature estimates. The obtained estimates for the temperature correspond to an intermediate temperature between chromospheric temperatures (10^4 K) and transition region temperatures (10^5 K). Cospatial emission with dark thread is observed in the 1600 Å channel,

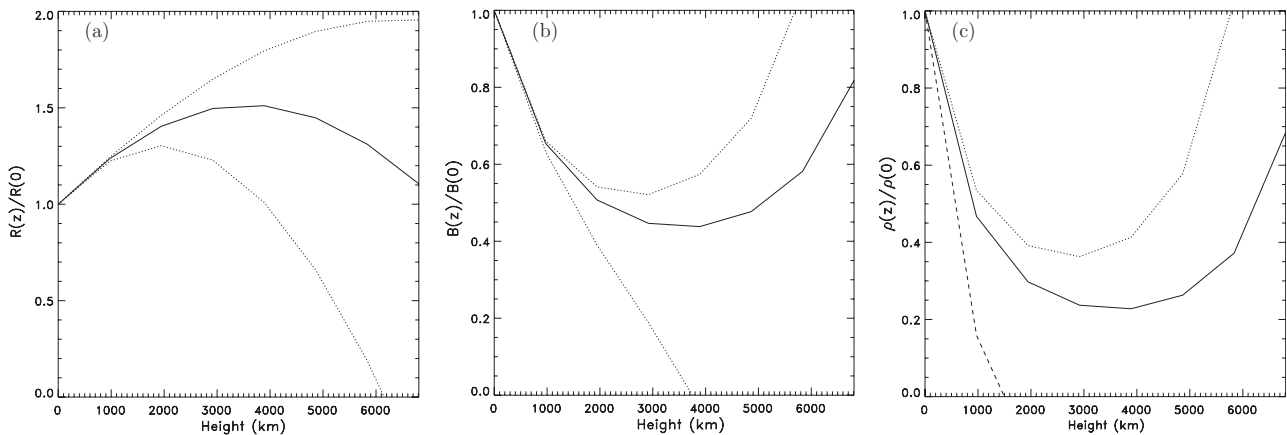


Figure 8. (a) Estimated expansion of the flux tube (solid line) along the dark thread derived by means of magnetoseismology. The dashed lines correspond to the 95% confidence interval. (b) The estimated change of magnetic field strength (solid line) along the dark thread from magnetoseismology. The dashed lines correspond to the 95% confidence interval. (c) The estimated change in density (solid line) along the dark thread obtained by solar magnetoseismology. The short dashed line corresponds to the 95% confidence interval, whereas the long dashed line corresponds to a 70% confidence interval.

which has contributions from transition region elements (i.e., C IV). Investigation of the emission reveals that it appears to be transition region material associated with, rather than part of, the ejection of the dark thread. This suggests that the material is at least cooler than the transition region plasma, i.e., $T < 10^5$ K.

As we see signals of a reconnection event, this could suggest that the thread is a chromospheric loop that has been heated. The obtained estimates of temperature also agrees with the hypothesis given by our earlier arguments on why the filament appears dark in the 171 Å channel, furthering credence to the suggestion that we see a similar event to Liu et al. (2009). Further, the obtained estimates for the density scale height are greater than the estimated scale heights derived for spicules from magnetoseismology in Verth et al. (2011) because the thread is hotter than Ca II H spicules.

4.2. Estimation of Flux Tube Expansion

Now, the rest of the phase travel times occur during times of significant dynamic behavior in the larger jet (see Figure 2). We do not know if the dark thread also experiences similar dynamic behavior. To make progress, we assume the thread is at least in a quasi-static state during the time for which the position of the maximum amplitude of the wave propagates through the cross-cuts. This means that the following magnetoseismological results can be interpreted as a time average of the thread's structure.

The phase travel time for the position of the maximum amplitude has a very similar fit when either a quadratic or exponential fit is used. We use an exponential fit since this is particularly convenient for calculating the uncertainty in the rate of change of phase speed along the thread. This is necessary for quantifying the uncertainty in magnetic field strength and plasma density gradients inferred from the following magnetoseismology. In Figure 7(a), the measured phase speed is shown and in Figure 7(b) we plot the measured phase speed minus the flow, i.e., what should be the actual phase speed of the wave, for the position of the maximum amplitude.

Using Equation (7), it is obvious that we can write

$$\frac{R}{R_0} = \sqrt{\frac{c_{k0}}{c_k} \frac{\xi_\perp}{\xi_{\perp 0}}}, \quad (12)$$

where $\xi_{\perp 0}$ and R_0 are the values obtained at lowest height and ξ_\perp and R are the values obtained at a greater height. Using the

measured value of amplitude and the actual phase speed, we can determine the rate of flux tube expansion. Figure 8(a) shows the normalized expansion along the dark thread.

What likely values of expansion should we expect for the dark thread? It is possible, as mentioned, that the dark thread will display the same behavior as the larger UV/EUV jet. The local expansion with height of the dark thread is initially similar to that measured in the global jet structure shown in Figure 2(a). The large UV/EUV jet takes on the shape of a magnetic funnel, suggested as being the standard magnetic configuration for the quiet Sun (e.g., Gabriel 1976; Peter 2001). Expected expansion factors from extrapolations for quiet-Sun magnetic funnels, e.g., Tan et al. (2010), are 4–12 for heights less than 20 Mm and 1–3 for heights greater than 20 Mm. The calculated expansion in Figure 8(a) also appears to show the dark thread exhibiting a contraction of the cross-sectional area, with the profile being almost symmetric about 3500 km. Is it possible this is a real contraction? Two likely scenarios suggest themselves if it is a real contraction: (1) if the thread is a chromospheric loop and reconnection occurred close to a footpoint of the loop, then we may expect the dark thread to have a relatively symmetric profile about the apex; (2) there are strong magnetic elements either side of the dark thread forcing the field lines to converge. However, the results from the previous section suggest the density is decreasing along the dark thread. It is possible this contraction has disappeared (due to untwisting of the thread) between the time the maximum amplitude travels along the thread to the time the second minimum travels. The decreasing flow speed may be a sign that the thread has untwisted/opened up significantly between these two events. However, the minimum amplitude also appears to show a decrease of amplitude with height.

Another option is that the kink wave experiences damping. Resonant absorption is known to be an efficient method for the damping of propagating kink waves (e.g., Terradas et al. 2010; Goossens et al. 2011) and is an ideal candidate for plasma heating (Erdélyi 1998; Taroyan & Erdélyi 2009). Also, dynamic behavior has been shown to attenuate/amplify the amplitudes of MHD waves (Morton & Erdélyi 2009b; Morton et al. 2010; Ruderman 2010; Erdélyi et al. 2011). This means the contraction would be an artifact as the oscillation is damped. We can estimate the wavelength/wavenumber of the kink wave. The typical period of the oscillations (e.g., see oscillation in Figure 5) is 360 s. Using $P = 2\pi/\omega$ then, $5400 < \lambda < 18,000$ km and $5 \times 10^{-5} < k < 25 \times 10^{-4}$ km $^{-1}$ for $15 < c_k < 50$ km s $^{-1}$.

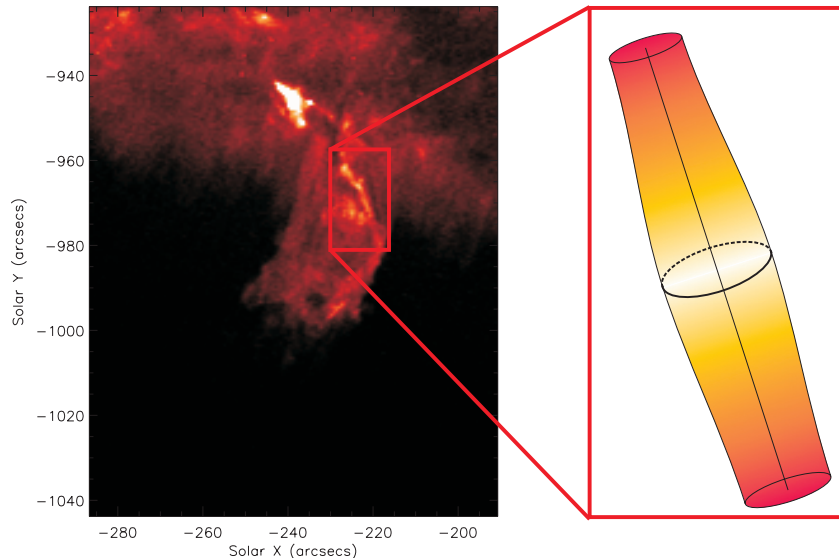


Figure 9. Schematic representation of the sub-resolution features of the dark thread determined from magnetoseismology.
(A color version of this figure is available in the online journal.)

This means $0.03 < kR < 0.15$ for a radius of ~ 725 km (the radius is at resolution length scales) and resonant damping is efficient at these wavelengths.

We can also determine the magnetic and density gradients along the dark thread. The magnetic field varies as

$$B(z) \propto \frac{1}{R^2(z)},$$

and this is shown in Figure 8(b). Further, using the values of the actual phase speed and the relation

$$\rho \propto \frac{B^2}{c_k^2}$$

we can determine the density gradient, Figure 8(c). If we fit a decreasing exponential profile to the decreasing section of the density we obtain a scale height of $H \sim 1.2$ Mm and thread temperature of $T \sim 2.6 \times 10^4$ K. This temperature is less than the estimates obtained in the previous subsection and adds weight to the suggestion the thread is chromospheric in origin. Note, the reason for a 70% confidence interval in Figure 8(c) rather than a 95% interval is due being unable to calculate higher confidence due to large relative errors on the density.

In Figure 9, we provide a schematic representation of the apparent scenario in the jet suggested by the magnetoseismology. It demonstrates the sub-resolution expansion of the thread and the density stratification that can be inferred from such an approach.

5. CONCLUSIONS

In the present study, we demonstrate the successful application of solar magnetoseismology to a solar jet. In particular, we determine information on various plasma parameters of a dark thread that is observed to occur with a UV/EUV solar jet. From the magnetoseismology we are able to estimate the temperature of the dark thread, the sub-resolution expansion and the magnetic and density gradients along the thread. It would be difficult to obtain this information through analysis of the *SDO/AIA* filter data or spectral lines profiles, e.g., Stokes profiles, line widths, etc.

The nature of the dark thread is still a mystery as no similar feature has been reported previously. The temperature estimates ($T \sim 3 \times 10^4$) obtained from the magnetoseismology suggest the plasma is cooler than the observable temperature ranges of both the 304 Å and 171 Å. This is probably the reason, along with the plasma being optically thick/dense, that the thread appears as a dark inclusion in the filters. A dense, $T \sim 3 \times 10^4$, plasma is likely to have originated in the chromosphere. The thread feature is possibly part of an emerging flux region that was responsible for the reconnection that caused the jet. The closest comparison we find is the chromospheric jet observed by Liu et al. (2009, 2011).

With respect to the magnetoseismology, the fact we obtain reasonable temperature estimates for the plasma gives confidence that the density and magnetic field gradients also obtained are physical. The only issue that arises is the apparent contraction with height of the loop. A reasonable scenario that fits with the entire picture of the jet and the other results from the seismology is difficult to come by. It could be due to having neglected any influence of wave damping (e.g., due to resonant absorption) or because we are missing information on the dynamic evolution of the dark thread. Further theoretical studies into the influence of dynamic plasma behavior on wave propagation are required if a full picture of an object's dynamic behavior is to be found via magnetoseismology alone.

The authors thank A. Engell, D. Jess, and P. Grigis for a number of useful discussions. R.E. acknowledges M. Kéray for patient encouragement. The authors are also grateful to NSF, Hungary (OTKA, Ref. No. K83133) and the Science and Technology Facilities Council (STFC), UK for the financial and IDL support they received. The data are provided courtesy of NASA/*SDO* and the AIA, EVE, and HMI science teams. The *STEREO/SECCHI* data used here were produced by an international consortium of the Naval Research Lab, Lockheed Martin Solar and Astrophysics Lab, NASA Goddard Space Flight Center (USA), Rutherford Appleton Laboratory, University of Birmingham (UK), Max-Planck Institut for Solar System Research (Germany), Center Spatial de Liège (Belgium), Institut

d'Optique Théorique et Appliquée, and Institut d'Astrophysique Spatiale (France).

REFERENCES

- Andries, J., van Doorsselaere, T., Roberts, B., et al. 2009, *Space Sci. Rev.*, **149**, 3
- Aschwanden, M. J. 2004, Physics of the Solar Corona (Berlin: Springer)
- Banerjee, D., Erdélyi, R., Oliver, R., & O'Shea, E. 2007, *Sol. Phys.*, **246**, 3
- Bender, C. M., & Orszag, S. A. 1978, Advanced Mathematical Methods for Scientists and Engineers (New York: McGraw-Hill)
- Bohlin, J. D., Vogel, S. N., Purcell, J. D., et al. 1975, *ApJ*, **197**, L133
- Brueckner, G. E., & Bartoe, J.-D. F. 1983, *ApJ*, **272**, 329
- Centeno, R., Trujillo Bueno, J., & Asensio Ramos, A. 2010, *ApJ*, **708**, 1579
- Cirtain, J. W., Golub, L., Lundquist, L., et al. 2007, *Science*, **318**, 1580
- De Moortel, I. 2009, *Space Sci. Rev.*, **149**, 65
- Del Zanna, G., & Mason, H. E. 2003, *A&A*, **406**, 1089
- Erdélyi, R. 1998, *Sol. Phys.*, **180**, 213
- Erdélyi, R. 2006a, *Phil. Trans. R. Soc. A*, **364**, 351
- Erdélyi, R. 2006b, in Proc. SOHO 18/GONG 2006/HELAS I, Beyond the Spherical Sun, ed. K. Fletcher & M. Thompson (ESA SP-624; Noordwijk: ESA), 15
- Erdélyi, R., Al-Ghafri, K. S., & Morton, R. J. 2011, *Sol. Phys.*, **272**, 73
- Erdélyi, R., & Fedun, V. 2007, *Science*, **318**, 1572
- Gabriel, A. H. 1976, *Phil. Trans. R. Soc. A*, **281**, 339
- Goossens, M., Erdélyi, R., & Ruderman, M. S. 2011, *Space Sci. Rev.*, **158**, 289
- Harrison, R. A. 1999, Magnetic Fields and Solar Processes (ESA SP-448; Noordwijk: ESA), 531
- Howard, R. A., Moses, J. D., Vourlidas, A., et al. 2008, *Space Sci. Rev.*, **136**, 67
- Kamio, S., Curdt, W., Teriaca, L., Inhester, B., & Solanki, S. K. 2010, *A&A*, **510**, L1
- Lemen, J. R., Title, A. M., Akin, D. J., et al. 2011, *Sol. Phys.*, in press (doi:10.1007/s11207-011-9776-8)
- Liu, W., Berger, T. E., Title, A. M., & Tarbell, T. D. 2009, *ApJ*, **707**, L37
- Liu, W., Berger, T. E., Title, A. M., Tarbell, T. D., & Low, B. C. 2011, *ApJ*, **728**, 103
- Morton, R., & Erdélyi, R. 2009a, *A&A*, **502**, 315
- Morton, R., & Erdélyi, R. 2009b, *ApJ*, **707**, 750
- Morton, R. J., & Erdélyi, R. 2010, *A&A*, **519**, 43
- Morton, R. J., Hood, A. W., & Erdélyi, R. 2010, *A&A*, **512**, 23
- Newton, H. W. 1934, *MNRAS*, **94**, 472
- Pariat, E., Antiochos, S. K., & DeVore, C. R. 2009, *ApJ*, **691**, 61
- Patsourakos, S., Pariat, E., Vourlidas, A., Antiochos, S. K., & Wuelser, J. P. 2008, *ApJ*, **680**, L73
- Peter, H. 2001, *A&A*, **374**, 1108
- Pike, C. D., & Mason, H. E. 1998, *Sol. Phys.*, **182**, 333
- Pintér, B., Jain, R., Tripathi, D., & Isobe, H. 2008, *ApJ*, **680**, 1560
- Roberts, B., Edwin, P. M., & Benz, A. O. 1984, *ApJ*, **279**, 857
- Ruderman, M. S. 2010, *Sol. Phys.*, **267**, 377
- Ruderman, M. S., & Erdélyi, R. 2009, *Space Sci. Rev.*, **149**, 199
- Ruderman, M. S., Verth, G., & Erdélyi, R. 2008, *ApJ*, **686**, 694
- Shibata, K., Ishido, Y., Acton, L. W., et al. 1992, *PASJ*, **44**, L173
- Shibata, K., & Uchida, Y. 1985, *PASJ*, **37**, 31
- Shimojo, M., Hashimoto, S., Shibata, K., et al. 1996, *PASJ*, **48**, 123
- Soler, R., Arregui, I., Oliver, R., & Ballester, J. L. 2010, *ApJ*, **722**, 1778
- Soler, R., Oliver, R., & Ballester, J. L. 2009a, *ApJ*, **699**, 1553
- Soler, R., Oliver, R., & Ballester, J. L. 2009b, *ApJ*, **707**, 662
- Sterling, A. C., Harra, L. K., & Moore, R. L. 2010, *ApJ*, **722**, 1644
- Tan, B., Tian, H., & He, J. S. 2010, *Chinese Astron. Astrophys.*, **34**, 40
- Taroyan, Y., & Bradshaw, S. 2008, *A&A*, **481**, 247
- Taroyan, Y., & Erdélyi, R. 2009, *Space Sci. Rev.*, **149**, 229
- Terradas, J., Arregui, I., Verth, G., & Goossens, M. 2011, *ApJ*, **729**, L22
- Terradas, J., Goossens, M., & Verth, G. 2010, *A&A*, **524**, 23
- Uchida, Y. 1970, *PASJ*, **22**, 341
- Van Doorsselaere, T., Brady, C. S., Verwichte, E., & Nakariakov, V. M. 2008, *A&A*, **491**, L9
- Vasheghani Farahani, S., Van Doorsselaere, T., Verwichte, E., & Nakariakov, V. M. 2009, *A&A*, **498**, L29
- Verth, G., & Erdélyi, R. 2008, *A&A*, **486**, 1015
- Verth, G., Erdélyi, R., & Jess, D. B. 2008, *ApJ*, **687**, L45
- Verth, G., Goossens, M., & He, J.-S. 2011, *ApJ*, **733**, L15
- Verth, G., Terradas, J., & Goossens, M. 2010, *ApJ*, **718**, L102
- West, M. J., Zhukov, A. N., Dolla, L., & Rodriguez, L. 2011, *ApJ*, **730**, 122
- Winebarger, A. R., DeLuca, E. E., & Golub, L. 2001, *ApJ*, **553**, L81
- Yokoyama, T., & Shibata, K. 1995, *Nature*, **375**, 42
- Yokoyama, T., & Shibata, K. 1996, *PASJ*, **48**, 353
- Zaqarashvili, T. V., & Erdélyi, R. 2009, *Space Sci. Rev.*, **149**, 355